Inorg. Chem. **2004**, *43*, 3441–3446

Photocatalytic Synthesis of Copper Colloids from Cu(II) by the Ferrihydrite Core of Ferritin

Daniel Ensign,[†,‡] Mark Young,[‡,§] and Trevor Douglas*[,†,‡]

Department of Chemistry and Biochemistry, Department of Plant Sciences, and Center for Bio-Inspired Nanomaterials, Montana State University, Bozeman, Montana 59717

Received December 9, 2003

The iron-storage protein ferritin encapsulates a nanoparticle of iron oxide. The size and properties of these nanoparticles can be adjusted by controlled oxidative hydrolysis reactions of Fe(II). This mineralized ferritin protein cage has previously been shown to act as an effective photocatalyst for reduction of Cr(VI). In the present work, we demonstrate that Fe(O)OH-mineralized ferritin catalyzes the photoreduction of Cu(II) to form a stable, air-sensitive, colloidal dispersion of Cu(0). In addition, the particle sizes of the Cu colloids can be controlled by varying the ratio of Cu(II) to ferritin. This illustrates an important principle, namely that the properties of one preformed material can be utilized for the specific synthesis of a second material, thus tailoring the desired physical properties of the final products. This procedure represents a multistep materials synthesis: the formation of a new nanomaterial from a catalytic precursor.

Introduction

Biomimetic approaches to nanomaterials synthesis have provided a high degree of control over particle morphology, composition, and polymorph selection under relatively mild synthetic conditions.[1−3] In particular, protein cage architectures have successfully been used as size-constrained reaction environments to spatially limit nanoparticle growth or encapsulate preformed nanomaterials. These protein cage architectures include ferritin[4] and ferritin-like proteins,[5,6] lumazine synthase,[7] virus capsids,[8−10] and heat shock proteins.[11,12] The iron storage protein ferritin is widespread in biological systems, and self-assembles into either a 12- or 24-subunit cage-like architecture.[13,14] This protein cage surrounds a hollow cavity in which iron is sequestered and mineralized as a small particle of an iron oxyhydroxide (Fe(O)OH, ferrihydrite). The 24-subunit mammalian ferritins are roughly spherical protein cages with inner and outer diameters of 8 and 12 nm, respectively.[15,16] The native iron oxide particle may be easily removed from the protein cage by reduction of Fe(III) and subsequent chelation of Fe(II) to leave an empty, intact apo-protein cage. The empty protein cage of apoferritin has also been utilized as a size-constrained reaction vessel for the synthesis of several metal-oxide and -sulfide nanoparticles.[4,17−20] It is of interest to investigate

* To whom correspondence should be addressed. E-mail; tdouglas@chemistry.montana.edu.
† Department of Chemistry and Biochemistry.
‡ Center for Bio-Inspired Nanomaterials.
§ Department of Plant Sciences.

(1) Mann, S. *Biomimetic Materials Chemistry*; VCH Publishers: New York, 1996.
(2) Whaley, S. R.; English, D. S.; Hu, E. L.; Barbara, P. F.; Belcher, A. M. *Nature* **2000**, *405*, 665.
(3) Lee, S.-W.; Mao, C.; Flynn, C. E.; Belcher, A. M. *Science* **2002**, *296*, 892.
(4) Meldrum, F. C.; Wade, V. J.; Nimmo, D. L.; Heywood, B. R.; Mann, S. *Nature* **1991**, *349*, 684.
(5) Allen, M.; Willits, D.; Mosolf, J.; Young, M.; Douglas, T. *Adv. Mater.* **2002**, *14*, 1562.
(6) Allen, M.; Willits, D.; Young, M.; Douglas, T. *Inorg. Chem.* **2003**, *42*, 6300.
(7) Shenton, W.; Mann, S.; Colfen, H.; Bacher, A.; Fischer, M. *Angew. Chem., Int. Ed.* **2001**, *40*, 442.
(8) Douglas, T.; Young, M. J. *Nature* **1998**, *393*, 152.
(9) Douglas, T.; Strable, E.; Willits, D.; Aitouchen, A.; Libera, M.; Young, M. *Adv. Mater.* **2002**, *14*, 415.
(10) Dragnea, B.; Chen, C.; Kwak, E.-S.; Stein, B.; Kao, C. C. *J. Am. Chem. Soc.* **2003**, *125*, 6374.
(11) McMillan, R. A.; Paavola, C. D.; Howard, J.; Chan, S. L.; Zaluzec, N. J.; Trent, J. D. *Nat. Mater.* **2002**, *1*, 247.
(12) Flenniken, M. L.; Willits, D. A.; Brumfiled, S.; Young, M.; Douglas, T. *Nano Lett.* **2003**, *3*, 1573.
(13) Bozzi, M.; Mignogna, G.; Stefanini, S.; Barra, D.; Longhi, C.; Valenti, P.; Chiancone, E. *J. Biol. Chem.* **1997**, *272*, 3259.
(14) Lawson, D. M.; Artymiuk, P. J.; Yewdall, S. J.; Smith, J. M. A.; Livingstone, J. C.; Treffry, A.; Luzzago, A.; Levi, S.; Arosio, P.; Cesareni, G.; Thomas, C. D.; Shaw, W. V.; Harrison, P. M. *Nature* **1991**, *349*, 541.
(15) Harrison, P. M.; Arosio, P. *BBA Energetics* **1996**, *1275*, 161.
(16) Chasteen, N. D.; Harrison, P. M. *J. Struct. Biol.* **1999**, *126*, 182.
(17) Meldrum, F. C.; Heywood, B. R.; Mann, S. *Science* **1992**, *257*, 522.
(18) Hanfield, J. F. *Proc. Natl. Acad. Sci. U.S.A.* **1992**, *89*, 11064.

10.1021/ic035415a CCC: $27.50 © 2004 American Chemical Society
Published on Web 04/29/2004

thesynthesis and reactivity of these nanoparticles and develop new synthetic strategies for nanoparticle fabrication.

The iron oxide mineralized ferritin protein has been shown to act as a photocatalyst for redox transformations.[21,22] In these photochemical reactions, the ferric oxyhydroxide nanoparticle within the protein cage is thought to act as a visible-band-gap semiconductor. Upon photoexcitation, valence-band electrons are promoted to the conduction band, generating an electron−hole pair, which can be utilized to facilitate oxidation−reduction reactions. In the presence of sacrificial electron donors (e.g., organic acids such as tartrate or citrate), it has been shown that toxic species such as Cr(VI) can be efficiently reduced to Cr(III).[22] However, there is some uncertainty about the mechanism for this reaction. Direct contact between the substrate and the mineral would require entry of the anionic CrO_4^{2-} across an unfavorable electrostatic gradient.[23,24] Alternatively, photoinduced electron transfer through the 2-nm protein shell would be required to reduce CrO_4^{2-} on the exterior of the protein cage. Despite the mechanistic uncertainty, the mineralized iron oxide nanoparticle within the ferritin protein cage represents a powerful photocatalytic system, and details of the reaction mechanism are under investigation.

In the present work, we have used the inherent photocatalytic activity of the iron-oxide-mineralized ferritin for the formation of stable copper colloids by photoreduction of aqueous Cu(II). Metal clusters such as these have interesting optical, electronic, and catalytic properties not observed in bulk materials.[25−27] For instance, colloids of Cu, Ag, and Au manifest surface-enhanced Raman scattering effects,[28] and Au nanoparticles show size-dependent behavior toward CO oxidation.[29] Previous syntheses of Cu nanoparticles have used reverse micelles,[30−32] organometallic precursors,[33] and relatively harsh synthetic conditions.[30−34] In contrast, the photocatalytic activity of the iron-oxide-mineralized ferritin system has allowed us to use visible light for the synthesis of Cu nanoparticles under mild aqueous conditions. The resulting materials have been characterized by UV−vis spectroscopy, dynamic light scattering, transmission electron microscopy, electron energy-loss spectroscopy, and electron diffraction.

Experimental Section

Apoferritin (Sigma) was mineralized with Fe(O)OH in order to control the size and concentration of iron oxide cores used in the photolysis reactions. To this end, aliquots of 25.5 mM deaerated $(NH_4)_2Fe(SO_4)_2{\cdot}6H_2O$ (Aldrich, 99+%) were added to a 5 mL solution of apoferritin (10 mg, 0.01 μmol), buffered at pH 6.2 (25 mM MES: Sigma, 99.5%; 25 mM NaCl: Fischer). One 392-μL aliquot of $(NH_4)_2Fe(SO_4)_2{\cdot}6H_2O$ gave a theoretical loading of 500 Fe per protein; two gave a loading of 1000 Fe per protein. Solutions were then allowed to react at 4 °C for 12 h. The mineralized ferritin was subsequently purified by size exclusion chromatography, resulting in a protein concentration of 1 mg/mL as determined using the biuret method. The protein was then dialyzed into 125 mM NaCl.

For photolysis, a solution of 125 mM HEPES (Fischer, 99%) and 400 mM sodium citrate (Fischer) or potassium sodium tartrate (Aldrich, 99%) (pH 7.3) was prepared. An 800-μL sample of protein solution was combined with 100 μL buffer solution in a semi-micro UV-transparent cuvette. Loadings of 2000, 1000, 500, or 250 copper atoms per cage were obtained by adding 100, 50, 25, or 13 μL of a 40-mM solution of $CuSO_4{\cdot}5H_2O$ (Aldrich, 99.995%); deionized water was added to increase the final solution volume to 1.0 mL. Solutions were illuminated using a Xe arc lamp (175 W, Lambda-LS, Sutter Instruments). IR radiation was removed by passing the beam through a water filter, while a jacketed cuvette and circulating water bath served to maintain the temperature of samples at 4 °C.

Reactions with Cu(II) loadings of 2000, 1000, 500, and 250 Cu atoms per ferritin at a fixed iron loading of 1000 Fe atoms per ferritin were followed spectroscopically (Agilent 8453) in the visible region, in particular the increase in absorbance at 570 nm. The reaction was monitored at two Fe loadings (1000 and 500 Fe per ferritin) in the same manner.

Cu oxidation state was determined by using Cu(I)- and Cu(II)-specific indicators. A 100-μL portion of sample solution was combined with 100 μL of the Cu(I)-specific indicator bathocuproinedisulfonic acid (BCDSA, 10 mM; Aldrich, ~90%) and diluted with water to 1 mL, and the absorbance was measured at 480 nm.[35] The Cu(II)-specific porphine 5,10,15,20-tetrakis{4-[*N*-(trimethyl)-ammonio]phenyl}-21*H*,23*H*-porphine, tetrakis(*p*-toluenesulfonate) (TTMAPP; Aldrich, 98.5%) was used to detect Cu(II).[36] To this end, 10 μL of oxidized solution was added to 10 μL of porphine (10 mM) and diluted to 1 mL. The Cu(II)/TTMAPP complex was monitored at 432 nm.

Several analytical techniques were used to characterize the photoreaction products. Dynamic light scattering (DLS, Brookhaven 90Plus Particle Size Analyzer) yielded particle diameters at Cu(II)/ferritin ratios of 2000, 1000, and 500. The data were fit using a non-negatively constrained least-squares analysis.[37] The particles were visualized by TEM (LEO 912, 100 kV; and Zeiss 100C, 60 kV) immediately after photolysis. Samples were prepared by placing 5 μL of the sample solution on Formvar/carbon-coated copper EM grids. Particle sizes were measured by TEM and size distributions determined by a Gaussian fit of the data. The electron energy-loss spectroscopic capability of the LEO 912 was used to probe particle composition. Selected-area electron diffraction data (LEO 912, 100 kV; and Zeiss 100C, 80 kV) were collected on samples washed with deaerated water. A colloidal gold standard was used for calibration.

(19) Douglas, T.; Dickson, D. P. E.; Betteridge, S.; Charnock, J.; Garner, C. D.; Mann, S. *Science* **1995**, *269*, 54.
(20) Meldrum, F. C.; Douglas, T.; Levi, S.; Arosio, P.; Mann, S. *J. Inorg. Biochem.* **1995**, *58*, 59.
(21) Nikandrov, V. V.; Gratzel, C. K.; Moser, J. E.; Gratzel, M. *J. Photochem. Photobiol., B* **1997**, *41*, 83.
(22) Kim, I.; Hosein, H.-A.; Strongin, D. R.; Douglas, T. *Chem. Mater.* **2002**, *14*, 4874.
(23) Douglas, T.; Ripoll, D. R. *Protein Sci.* **1998**, *7*, 1083.
(24) Yang, X.; Arosio, P.; Chasteen, N. D. *Biophys. J.* **2000**, *78*, 2049.
(25) Henglein, A. *Chem. Rev.* **1989**, *89*, 1861.
(26) Hache, F., Ricard, D.; Flytzanis, C. *J. Opt. Soc. Am. B* **1986**, *3*, 1647.
(27) Stucky, G. D.; MacDougall, J. E. *Science* **1990**, *247*, 669.
(28) Creighton, J. A.; Eadon, D. G. *J. Chem. Soc., Faraday Trans.* **1991**, *87*, 3881.
(29) Chusuei, C. C.; Lai, X.; Luo, K.; Goodman, D. W. *Top. Catal.* **2001**, *14*, 71.
(30) Lisiecki, I.; Pileni, M. P. *J. Am. Chem. Soc.* **1993**, *115*, 3887.
(31) Lisiecki, I.; Pileni, M. P. *J. Phys. Chem.* **1995**, *99*, 5077.
(32) Lisiecki, I.; Billoudet, F.; Pileni, M. P. *J. Mol. Liq.* **1997**, *72*, 251.
(33) Bunge, S. D.; Boyle, T. J.; Headley, T. J. *Nano Lett.* **2003**, *3*, 901.
(34) Kapoor, S.; Joshi, R.; Mukherjee, T. *Chem. Phys. Lett.* **2002**, *354*, 443.
(35) Faizullah, A. T.; Townshend, A. *Anal. Chim. Acta* **1985**, *172*, 291.
(36) Makino, T.; Itoh, J. I. *Clin. Chim. Acta* **1981**, *111*, 1.
(37) Finsy, R. *Adv. Colloid Interface Sci.* **1994**, *52*, 79.

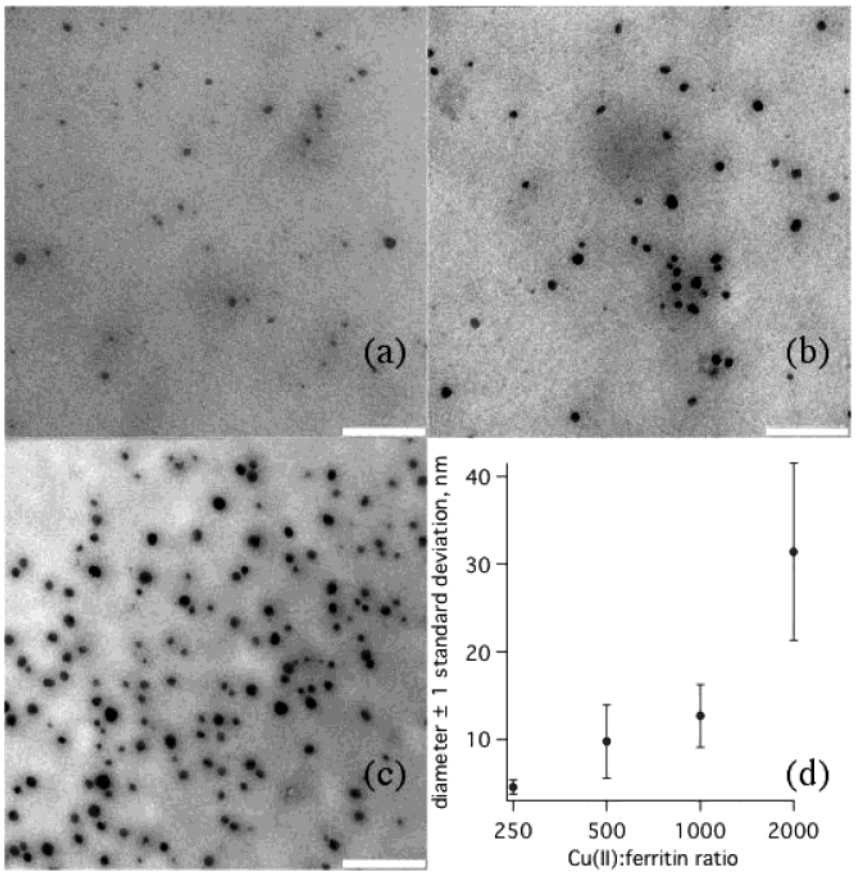

Figure 1. TEMs of product of photolysis of Cu(II) in the presence of ferritin (scale bars = 200 nm): (a) 500 Cu/ferritin, (b) 1000 Cu/ferritin, and (c) 2000 Cu/ferritin. (d) Particle sizes as measured using TEM. Mean (μ) and standard deviation (σ) values for the Gaussian fits across four different loadings of copper to protein are 250 Cu/ferritin, $\mu = 4.5$ nm, $\sigma = 0.8$ nm; 500 Cu/ferritin, $\mu = 9.7$ nm, $\sigma = 4.2$ nm; 1000 Cu/ferritin, $\mu = 12.7$ nm, $\sigma = 3.6$ nm; and 2000 Cu/ferritin, $\mu = 31.4$ nm, $\sigma = 10.1$ nm.

Results and Discussion

The photolysis of Cu(II) in the presence of iron-oxide-mineralized ferritin and a sacrificial reductant (citrate, tartrate) resulted in the formation of a wine-red color after an hour. Control reactions photolyzed in the absence of Cu(II), tartrate/citrate, or iron-oxide-mineralized ferritin did not change color over the same period. No reaction was observed when solutions were left in the dark or in the presence of the unmineralized (apo) ferritin. In addition, Fe(II) alone was not observed to spontaneously reduce Cu(II) in deaerated solutions.

Examination of the photolysis products by transmission electron microscopy (TEM) revealed electron-dense spheroid particles (Figure 1a−c), with the Cu(II)/ferritin ratio serving as the major determinant of particle size (Figure 1d). Histograms of particle sizes were fit to Gaussian distributions. Higher Cu(II)/ferritin ratios led to larger particle sizes, with loadings of 250, 500, 1000, and 2000 leading to average particle diameters of 4.5 ± 0.8, 9.7 ± 4.2, 12.7 ± 3.6, and 31.4 ± 10.1 nm, respectively.

Dynamic light scattering (DLS) of the starting material, prior to photolysis, revealed the presence of 12-nm diameter proteins as expected from the known dimensions of ferritin.[15,16] After photolysis, the photoreduction products were interrogated by DLS, and particles with average diameter 36 ± 3 nm for the 2000-Cu reaction (Figure 2), 28 ± 5 nm for the 1000-Cu reaction, and 16 ± 4 nm for the 500-Cu reaction were observed (Supporting Information). These particle sizes indicate that the products of reaction are individual colloidal particles, without extensive aggregation, and the diameters are in reasonable agreement with those measured by microscopy.

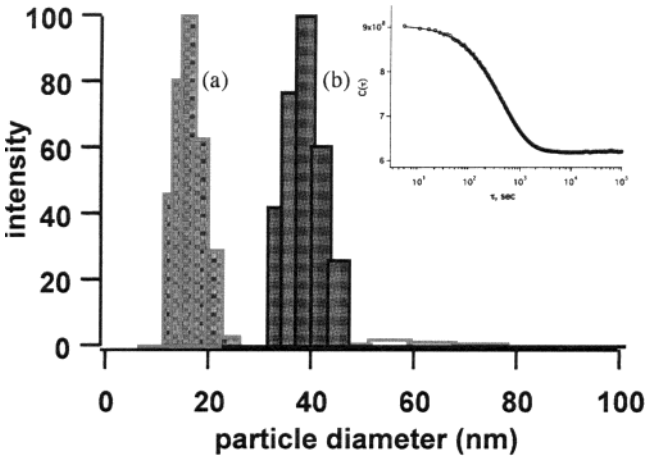

Figure 2. Dynamic light scattering of Cu nanoparticles (a) before and (b) after photolysis of Cu(II) solutions in the presence of mineralized ferritin. The inset shows the correlation function and fit for b.

The Cu particle dimensions as measured by TEM and DLS are larger than the intact 12-nm cage of ferritin. This suggests

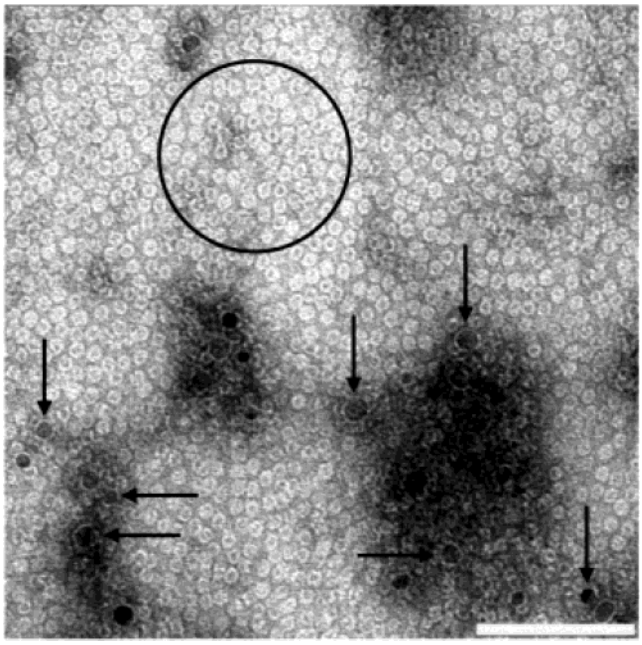

Figure 3. TEM of copper nanoparticles subjected to negative stain with uranyl acetate. The arrows indicate particles of Cu(0), surrounded by electron-transparent haloes, presumably protein. The circle indicates a typical area of negatively stained ferritin cages. (Scale bar = 200 nm.)

that the formation of Cu nanoparticles could either occur outside the protein cage, or that the protein cage is disrupted during formation of the Cu colloid within the protein, as has been previously suggested in the ferritin-constrained mineralization of U(VI) salts.[18] Negative stain TEM of the reaction product (2000 Cu(II)/ferritin) revealed that some of the Cu particles were surrounded by an electron-transparent layer, possibly protein (Figure 3), which is consistent with formation of the colloid within the confines of the protein cage. This indicates that the Cu-mineralized ferritin cages are severely expanded relative to the dimensions of the empty cage, but it suggests that the growth of the metallic nanoparticle could be at least partially limited by constraints imposed by the dimensions of the protein.

Using the electron energy-loss capability of the Leo 912 TEM, the copper L3,2 edges (944 eV, 996 eV) were observed from a collection of particles (Figure 4a), confirming the composition of the electron-dense particles.[38] Spectra collected from regions of the microscope grid without particles showed no Cu signal. Corresponding selected-area electron diffraction patterns of the copper colloid, after washing with deaerated water, revealed a powder diffraction pattern (Figure 4b) with *d*-spacings measured at 2.087, 1.807, 1.278, and 1.090 Å, consistent with the (111), (002), (022), and (311) reflections of FCC Cu metal.[33] These data exclude CuO or Cu_2O as major constituents of the nanoparticles.

The red color observed in this reaction is consistent with the formation of colloidal copper metal, Cu(0), confirmed

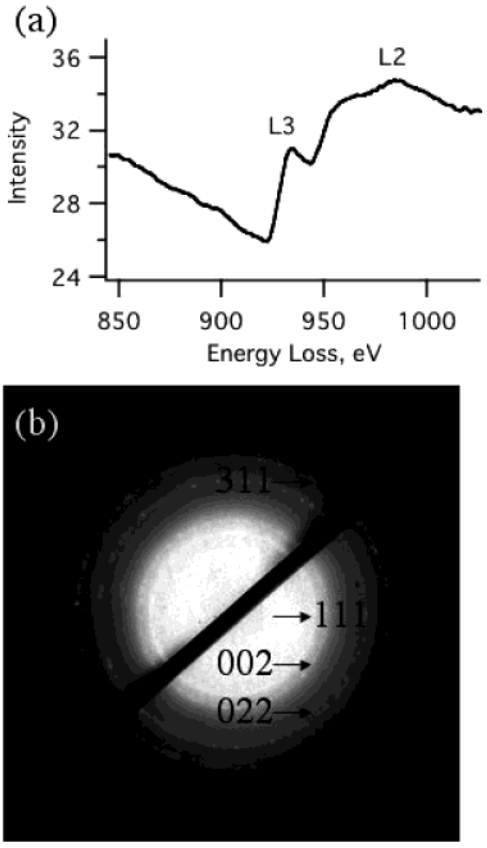

Figure 4. (a) Electron energy-loss spectrum of Cu particles formed after photolysis of Cu(II) in the presence of ferritin. The Cu L3 and L2 edges were measured to be 944 and 996 eV, respectively. (b) Selected-area electron powder diffraction pattern of copper colloids. The (111), (002), (022), and (311) reflections are visible.

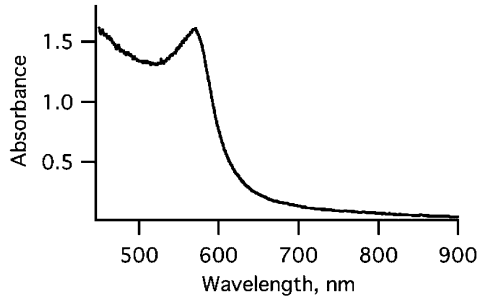

Figure 5. UV−vis absorbance spectrum of Cu(II) solutions photolyzed in the presence of mineralized ferritin, showing the absorbance maximum at 570 nm.

by electron diffraction data. This color is associated with a broad UV absorbance and an absorbance maximum at 570 nm (Figure 5) in the visible region. Creighton and Eadon[28] have calculated the absorption spectra for metallic colloids of many elements, including copper, and the calculated spectrum is remarkably similar to that measured during the photolysis reaction. The absorbance maximum at 570 nm has been ascribed to a plasmon resonance, although this is an incomplete description.[28] As noted by others, the position of the absorbance maximum is relatively insensitive to particle diameter within this size regime,[39,40] and only small (<5 nm) shifts are observed over the course of the reaction.

(38) Reimer, L.; Zepke, U.; Moesch, J.; Schulze-Hillert, S.; Ross-Messemer, M.; Probst, W.; Weimer, E. *EELSpectroscopy: A Reference Handbook of Standard Data for Indentification and Interpretation of Electron Energy-Loss Spectra and for Generation of Electron Spectroscopic Images*; Carl Zeiss, Electron Optics Division: Oberkoden, Germany, 1992.

(39) Yeh, M.-S.; Yang, Y.-S.; Lee, Y.-P.; Lee, H.-F.; Yeh, Y.-H.; Yeh, C.-S. *J. Phys. Chem. B* **1999**, *103*, 6851.

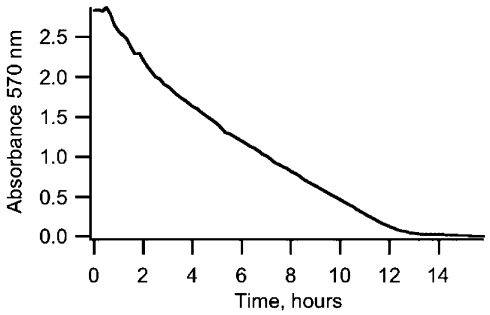

Figure 6. Air oxidation of Cu colloid as measured by the decrease in the absorbance maximum at 570 nm over several hours. The colloid appears to have oxidized completely after ~14 h.

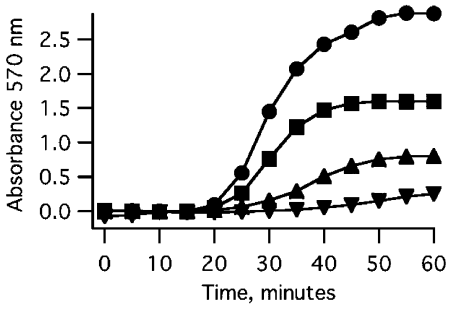

Figure 7. Change in absorbance at 570 nm for photolysis reactions across Cu(II) concentrations. All reactions had ferritin particles loaded with 1000 Fe (■, 2000 Cu per cage; ●, 1000 Cu per cage; ▲, 500 Cu per cage; ▼, 250 Cu per cage).

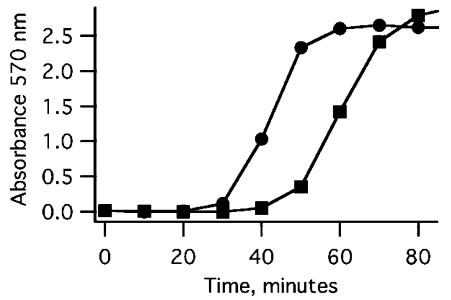

Figure 8. Effect of Fe loading on reaction rate, monitored by the absorbance maximum at 570 nm; the total iron content of both reactions was the same (●, photolysis with 2 mg/mL ferritin loaded with 500 Fe per cage; ■, photolysis with 1 mg/mL ferritin loaded with 1000 Fe per cage).

The spectroscopic signature of this plasmon peak suggests that the colloid is composed of fully reduced Cu rather than Cu_2O or CuO. This was chemically confirmed by the addition of the reducing agent sodium borohydride (Aldrich, 98%) to the red solutions, which revealed no noticeable change in the absorption spectrum. This implies that the Cu is in a fully reduced state. However, addition of hydrogen peroxide (EM Science, 30% solution) to the red solutions of the Cu colloid bleached the red color within minutes. The Cu(0) oxidation with H_2O_2 proceeded through a Cu(I) intermediate, which could be detected as a complex with bathocuproinedisulfonic acid (BCDSA). The addition of BCDSA to H_2O_2-oxidized solutions revealed a prominent absorption at 480 nm, characteristic of Cu(I)−BCDSA. The oxidation continued, and within 12 h, only the presence of Cu(II) could be detected by reaction with the Cu(II)-specific porphine indicator (TTMAPP).

The red color of solutions prepared by photoreduction also disappears when left open to air. However, the red color of the Cu colloid persists if the sample is kept under a positive pressure of nitrogen. Figure 6 shows the reoxidation of the colloid as monitored by the decrease of the 570-nm absorbance maximum for a solution with iron and copper loadings of 1000 and 2000 atoms per cage, respectively. Upon air oxidation of the Cu(0) colloid, the solutions had a yellow color. The materials giving rise to the yellow color of the solutions were not retained by 100-kDa ultrafiltration membranes, indicating that the yellow species was not associated with the ferritin protein (which is retained by these membranes). The yellow, oxidized solutions were examined to distinguish the presence of Cu(I) from Cu(II) using BCDSA and TTMAPP. In samples tested less than 1 day after the air oxidation of the colloid, the assays showed the presence of both Cu(I) and Cu(II). In samples which had been stored at 4 °C for two weeks, there was no detectable Cu(I), and only Cu(II) was present, suggesting that the copper colloid was oxidized to Cu(II) through a Cu(I) intermediate.

Oxidized solutions could be rephotolyzed, resulting in the formation of the same red color with the same absorbance spectrum and a particle size distribution (as measured by TEM) identical to that of the initial photolysis. Solutions have been subjected to up to three cycles of photolysis−oxidation, with no obvious change in the rate of appearance or size of the resulting Cu colloid. Upon reoxidation of the Cu(0) colloid, some disassembled ferritin protein was observed by size exclusion chromatography (SEC). Each subsequent reduction/oxidation cycle resulted in the formation of more disassembled protein cages when analyzed by SEC. However, TEM of these oxidized solutions clearly show the presence of assembled ferritin protein cages as the major component. SDS polyacrylamide gel electrophoresis of the oxidized material showed ferritin protein bands identical to apoferritin and mineralized ferritin starting materials, which implies that while the protein suffers some disassembly upon Cu nanoparticle formation, the subunits are not hydrolytically cleaved.

The reaction rates with respect to [Cu(II)] were measured spectroscopically by following the change in absorbance at 570 nm. These data are shown in Figure 7 for Cu(II) loadings of 2000, 1000, 500, and 250 Cu atoms per ferritin at a fixed iron loading of 1000 Fe atoms per ferritin. The rate of reaction is first order with respect to [Cu(II)] when calculated using the slope for the steepest portions of the traces, with a rate constant of 1.6×10^{-4} min^{-1}. To distinguish the effect of iron loading on the reaction rate, the photoreaction was monitored using ferritin particles loaded with either 500 or 1000 iron atoms per protein cage. Transmission electron micrographs of ferritin molecules loaded with 500 iron atoms per cage reveal smaller particles than those associated with ferritin with 1000 Fe per cage.[41] The efficiencies of the 500-

(40) Magruder, R. H.; Haglund, R. F.; Yang, L.; Wittig, J. E.; Zuhr, R. A. *J. Appl. Phys.* **1994**, *76*, 708.

(41) Gider, S.; Awschalom, D. D.; Douglas, T.; Mann, S.; Charparala, M. *Science* **1995**, *268*, 77.

and 1000-iron loadings were compared in the Cu(II) photoreduction reaction. Reactions with 2 mg/mL ferritin at 500 Fe loading and 1 mg/mL ferritin at 1000 Fe loading (Figure 8) and relative Cu(II) loading of 1000 (data not shown) and 2000 atoms per protein cage were compared. Under these conditions, all reactions contained the same total amount of Fe, but it appeared that the smaller (500-Fe) cores were more effective at catalyzing the reduction process. This is almost certainly due to the fact that twice as many ferritin molecules and associated iron oxide nanoparticle cores were present in this solution. In addition, the increased relative surface area of the smaller 500-Fe nanoparticles in this reaction may be an important kinetic effect which enhances the reaction rate.

The kinetic plots (Figures 7 and 8) exhibit sigmoidal shapes, suggestive of a mechanism for the Cu(II) reduction reaction that parallels the Fe(II) oxidation by ferritin. In the case of Fe mineralization in L-chain ferritin, having no ferroxidase sites, the process is rate limited by nucleation. After an initial slow lag phase, during which nucleation occurs, the mineralization reaction occurs quickly, as the oxidative hydrolysis is autocatalyzed by the growing mineral surface.[16] A similar process is suggested to occur in the formation of our Cu colloids; a slow nucleation step (reaction 1), followed by fast particle growth (reaction 2) as represented by the logarithmic portions of the kinetic plots. The similar charge/size ratio of Cu(II) and Fe(II) implies facile Cu(II) entry into the protein cage, equivalent to the electrostatically driven Fe(II) entry mechanism.[23] The growth of the Cu(0) core is not fully constrained by the interior dimensions of ferritin, leading to particles larger than 8 nm, and disruption of the protein cage. Interestingly, Cu ions are not found incorporated in ferritin mineral cores in vivo, so this has no real biological sugnificance, and Cu is tightly controlled in living cells and thus never appears as free aqua ions.[42]

$$Cu^{2+}_{(inside)} \rightarrow Cu^{0}_{(s)} \quad (1)$$

$$Cu^{2+}_{(inside)} + Cu^{0}_{(s)} \rightarrow Cu_{n}{}^{0}_{(s)} \quad (2)$$

Conclusion

The protein-constrained iron oxide mineral core of ferritin (ferrihydrite) is an effective catalyst for photoreduction reactions. We have shown that this system is capable of photoreduction of Cu(II) to form a colloidal dispersion of Cu(0) with a fairly narrow size distribution. This illustrates an important aspect of materials synthesis: that the properties of one preformed material can be utilized for the specific synthesis of a second material having different tailored physical properties. The ferritin system has previously shown itself to be a robust system for nanomaterials synthesis and an effective catalyst for photomediated redox transformations. Our present work opens a new horizon for the use of nanoparticle-mineralized ferritin as a photocatalyst for materials synthesis and provides a facile means for the preparation of metallic colloids. We are currently investigating variation in the composition and characteristics of the transition metal oxide cores of ferritin to fine-tune the properties of this novel photocatalyst and thus the range of catalytic reactions at our disposal.

Acknowledgment. The authors thank Sue Brumfield for assistance with transmission electron microscopy, and Mark Allen for assistance with electron diffraction. This work was funded in part by grants from EPA and the Petroleum Research Fund, administered by the American Chemical Society.

Supporting Information Available: Additional figures. This material is available free of charge via the Internet at http://pubs.acs.org.

IC035415A

(42) Luk, E.; Jensen, L. T.; Culotta, V. C. *J. Biol. Inorg. Chem.* **2003**, *8*, 803.